ISSN 2278-3091
Volume 9, No.1.5, 2020
International Journal of Advanced Trends in Computer Science and Engineering
Available Online at http://www.warse.org/IJATCSE/static/pdf/file/ijatcse0491.52020.pdf
https://doi.org/10.30534/ijatcse/2020/0491.52020

Optimization of Dual Band Two-Section Branch-Line Coupler with Nonuniform Impedances Using Surrogate-Based Method for 5G Applications

Ayyoub El Berbri[1], Adil Saadi[2], Seddik Bri [3]
[1,2] Modeling, Information Processing and Control Systems (MIPCS), National Graduate School of Arts and Crafts, Moulay Ismail University Meknes, Morocco , [1]ayyoub.elberbri@gmail.com
[3]Materials and Instrumentation, High School of Technology, Moulay Ismail University Meknes, Morocco

ABSTRACT
This paper presents an optimization of a Two-Section Dual-Band Branch-Line Coupler (BLC) with stepped-impedance-stub lines (SISL), that exploit the nonuniform impedances of the coupler branches. The optimization has been done using an adjusted optimization surrogate-based method. This enhanced BLC operates over n50 and n48 bands, that belongs to 5G NR frequency bands developed by 3GPP for the 5G (fifth generation) mobile network. The simulated results validate good dual-band performances at the two bands.

Key words: 5G, Branch-Line Coupler Dual-Band, Optimization,

1. INTRODUCTION

The growing demand for mobile communication is more than ever. For this reason, many researchers and developers around the world are engaged in the development of a new generation of communication. 5G NR (New Radio) is a new radio access technology (RAT) developed by 3GPP for the 5G (fifth generation) mobile network. It is supposed to be the global standard for the air interface of 5G networks. We use the two bands n50 and n48 from the latest published version of the 3GPP TS 38.101 [1].

Branch-line couplers offer a 90° phase difference and equal/unequal power splitting, which is useful in various microwave circuits, such as balanced mixers, data modulators, phase shifters, and power combined amplifiers [2]. Research has proposed various planar structures for a dual-band branch-line coupler design [3]-[9]. In this work, we use stepped-impedance-stub branches for both dual-band operation and compactness [10].

Simulation-driven design optimization and design closure have become an important part of contemporary microwave engineering. Still, they face the fundamental difficulty of the high computational cost of electromagnetic (EM) simulation. This cost may be prohibitive, particularly for complex structures. One of the solutions is co-simulation [11]. A truly efficient EM-based design optimization can be realized using surrogate models [12]. Probably the most successful approach of this kind in microwave engineering is space mapping (SM) [13] as well as various response correction techniques [14]. For a well-performing SM algorithm with a judiciously selected surrogate model, a satisfactory design is obtained only after a few (typically 3 to 10) full-wave EM simulations of the structure under consideration [13]. Further progress in terms of reducing the computational cost of the optimization process can be obtained using tuning space mapping (TSM): one of the latest and highly specialized developments in space mapping technology [15]. TSM combines SM with the concept of tuning.

This work presents an enhanced two-section BLC with SISL for dual-band operations, designed to perform for 5G NR frequency bands: n50= [1.432 GHz– 1.517 GHz] and n48= [3.55 GHz – 3.7 GHz]. This bands are developed by 3GPP for the 5G (fifth generation) mobile network [1]. The physical dimensions of this coupler are optimized to meet the design specifications using an adjusted Tuning Space Mapping, the adjustment is made in the tuning model using our engineering expertise and knowledge of the design problem. The simulated results of this enhanced two-section BLC show good dual-band performances at n50/n48.

2. ANALYSIS OF THE DUAL-BAND BLC

1.1 Single Section Dual-Band BLC

Designers typically construct traditional 3-dB branch-line couplers using λ/4 branches with impedances of 50 Ω and 50/√2. These branches have an electrical length of 90° at a single frequency that must be replaced for dual-band operation. Figure 1(a) presents the stepped impedance stub line, comprising a signal path (Z_3, θ_3) tapped with a stepped-impedance stub of (Z_1, θ_1) and (Z_2, θ_2) at its center. The advantages of this structure attribute to its increased nonuniform impedances, resulting in a compact size, wide range of realizable frequency ratio, and more realizable impedances. The stub line performs an equivalent electrical length of 90° and the desired branch impedances at two operating frequencies [10]. Figure 1(b) plots the coupler schematic with stepped-impedance-stub lines, where (θ_1, θ_2,

θ_3) the electrical lengths of the lines (1,2,3) respectively, and (Z_1, Z_2, Z_3) the impedances of the lines (1,2,3).

1.2 Two-Section Dual-Band BLC

In advanced communication systems, branch-line couplers not only require dual-band operation but also desire wide bandwidth. However, the single-section dual-band coupler only has a very narrow bandwidth. Fortunately, using multiple cascading sections improves the coupler. Since the dual-band

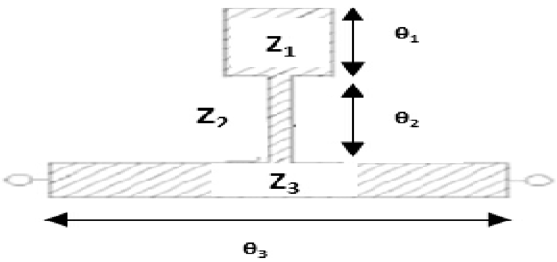

(a)

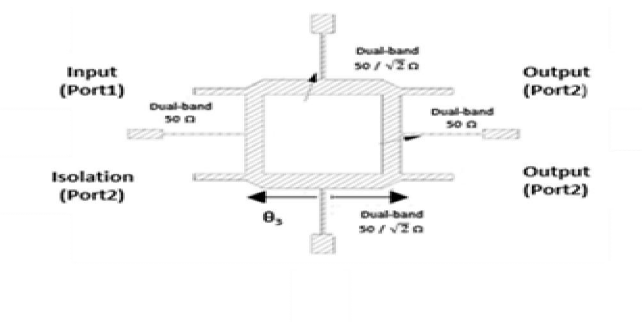

(b)

Figure 1 a: Proposed dualband stepped-impedance-stub branch line; **b**: Schematic of the dual-band single-section branch-line coupler with stepped-impedance-stub lines.

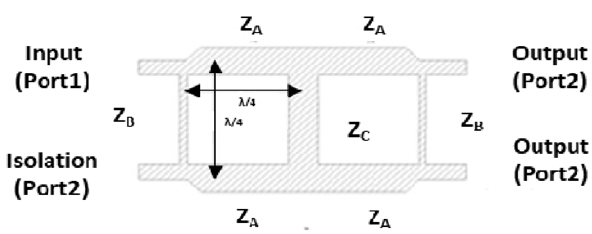

(a)

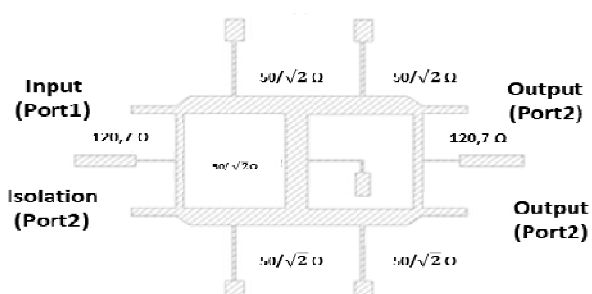

(b)

Figure 2: Configurations of: (a) a conventional two-section branch-line coupler (single band) and (b) the proposed dual-band two-section branch-line coupler with stepped-impedance stubs.

lines can be designed separately, the easy way for a two-section coupler design is to find required branch impedances first from the single-band synthesis equations, and then replace each with the corresponding dual-band stepped-impedance-stub line [10]. Figure 2.a shows the single-band BLC and Figure 2.b shows the two-section BLC, with the impedances (Z_A, Z_B, Z_C) and electrical lengths of $\lambda/4$.

Where Z_B=120.7 Ω and Z_A=Z_C=$\dfrac{50}{\sqrt{2}}\,\Omega$.

3. TUNING SPACE MAPPING ALGORITHM

3.1 EM-Simulator-Based Tuning

While the use of accurate but CPU-intensive EM simulation is now taken for granted by the microwave industry and computers are increasingly more powerful, microwave engineers are still faced with ever-larger design problems, tighter specifications, and shorter closure time requirements. Thus, design optimization processes based on full-wave EM simulations and validations will continue to remain challenging. The EM-simulator-based tuning method [16] is an effective tuning or design approach that combines EM accuracy with circuit speed. The approach allows easy tuning and instantaneous visualization of the EM-simulated responses of a structure. The heart of the method is the hybridization of EM simulation and circuit simulation in one structure (in our terminology a “tuning model”). It is achieved by replacing part of the EM-simulated structure (high-fidelity or “fine” model with physics-based equivalent circuit models or by suitable numerical approximations. Predefined physics-based models are preferable for their minimal sample data requirements.

3.2 Introduction to Tuning Space Mapping

Space mapping is one of the efficient optimization techniques [17,23]. It effectively exploits the surrogates of the fine model, surrogate models themselves are constructed from a so-called “coarse” model. They are of low fidelity but are much cheaper to evaluate than the fine model. Conventional space mapping techniques typically use purely circuit-based models or interpolated coarse-mesh EM models as surrogates.

Inspired by the EM-simulator-based tuning method, tuning space mapping technology is formulated [15]. Tuning space mapping algorithms exploit tuning models (EM-simulated model data or S-parameter files augmented by tuning elements) as surrogates. The surrogates approximate the full-wave EM simulation responses in an iterative space mapping updating process, essentially in the same way as do the conventional space mapping approaches. Tuning space mapping algorithms involve a fine model (e.g., a full-wave EM simulation), auxiliary fine models (fine models with tuning ports), a tuning model, and a calibration scheme that sometimes exploits an extra calibration (coarse) model. We may induce infinitesimal tuning gaps (negligible compared to the wavelength) into the fine model. We may then define tuning ports at the gap edges or at the boundary of the fine model to form candidate auxiliary fine models. We simulate the auxiliary models in an EM simulator and save the resulting multi-port S-parameter file. Within a circuit simulator, we insert or attach suitable tuning elements to the tuning ports. Preferably, the tuning elements are distributed circuit elements with physical dimensions corresponding to those of the fine model. This new tunable model bearing the EM-based S-parameter file data and tuning elements, namely, this new surrogate, is called a tuning model. After a simple alignment procedure (also known as parameter extraction or PE), we match the tuning model with the fine model. Some of the fine-model couplings are preserved (or represented through the S-parameter file) in the tuning model. We normally obtain a good surrogate of the fine model. In the next stage, the tuning model is optimized by varying the tuning parameter values of the tuning elements to satisfy given design specifications. Following a translation process, the resulting design parameter values constitute our next fine model iterate.

3.3 General Tuning Space Mapping Algorithm

The optimization statement for tuning space mapping is the same as for regular space mapping, namely [15].

$$x^*_f = \arg \min_{x_f \in X_f} U(R_f(x_f)) \tag{1}$$

Where $R_f : X_f \to R^m$ is the fine model response, $x_f : X_f \subseteq R^n$ is the fine model design parameters, x^*_f is the optimal fine model design, and U is a selected objective function.

We denote the design variable vector in the current iteration as

$x^{(i)}$ where i=0,1… $i = 0,1 \ldots$ is the index of the iteration. A typical tuning space mapping iteration consists of three steps: alignment, optimization and calibration.

Firstly, the current tuning model $R_t^{(i)}$ is built using fine model data at point $x^{(i)}$. In general, because the fine model has undergone a disturbance, the tuning model response may not agree with the response of the fine model at $x^{(i)}$ when the values of the tuning parameters $x_t^{(i)}$ are zero. In this case, an alignment process is needed to eliminate the mismatch through a slight adjustment of the tuning parameters. The alignment is implemented by conducting an optimization in the circuit simulator. It is formulated as:

$$x_{t,0}^{(i)} = \arg \min_{x_t} \left\| R_f(x^{(i)}) - R_t^{(i)}(x_i) \right\| \tag{2}$$

where $x_{t,0}^{(i)}$ is the adjusted tuning parameter after the alignment. In the next step, we optimize $R_t^{(i)}$ with respect to x_t to make it meet the design specifications. This is represented by

$$x_{t,1}^{(i)} = \arg \min_{x_t} U(R_t^{(i)}(x_t)) \tag{3}$$

where $x_{t,1}^{(i)}$ is the optimal tuning parameter. Just as in regular space mapping, the optimization process is conducted in fast circuit-theory-based simulators. The optimization goal is to meet the design specifications. However, in tuning space mapping, the optimization process is carried out with respect to the tuning parameters instead of the original design parameters.Then, we perform a calibration process to determine the desired adjustments of the design variables based on the optimal value of the tuning parameters. The calibration process, denoted as C, can be performed in various ways. To formulate this process, we firstly propose the following generic calibration equation.

$$x^{(i+1)} = C(x^{(i)}, x_{t,1}^{(i)}, x_{t,0}^{(i)}) \tag{4}$$

From this formula, we see that the calibration process produces a new design $x^{(i+1)}$ based on the previous design $x^{(i)}$, the adjusted tuning parameters $x_{t,0}^{(i)}$ obtained by the alignment process, and the optimal values of the tuning parameters $x_{t,1}^{(i)}$ gained from the optimization process.

4. RESULTS AND DISCUSSION

The dimensions of the single dual-band coupler have been computed using the synthesis equations of the single-band and dual-band [10]. The design parameters are x = $[L_1\ L_2]^T$ mm. The initial fine model as shown in Figure 3 is simulated using a substrate of ε_r = 4, height H =1.6 mm, and loss tangent=0.0004.

Figure 4 plots the initial fine model response, which shows S_{11} and S_{14} are below -10dB, from 3.4 GHz to 3.64 GHz, which not the entire band n48= [3.55 GHz – 3.7 GHz]. For better performance, optimization is needed.

The essential step is to construct the tuning model. Firstly, in the EM simulator we divide the fine model and insert co calibrated ports at the stubs Figure 5. The entire structure then simulated and the corresponding S16P data file is loaded into a 16-port S-parameter file component in a fast circuit simulator Figure 6. After that, appropriate circuit components are chosen and attached to the corresponding ports on this S-parameter component.

The tuning parameters $x_t = [L_{t1}\ L_{t2}]^T$ mm. The misalignment between the fine model response and the tuning model response with the tuning parameters set to zero is sufficiently small and can be ignored. Thus, an alignment process is not necessary and it is obvious that $x_{(t,0)}^{(0)}$ = $[0\ 0]^T$ mm.

The optimization process with respect to the tuning parameters is implemented in a fast circuit simulator Figure

6, which is aimed at satisfying the dual-band branch line coupler specifications. The tuning parameters obtained are $x_{(t,1)}^{(0)}$ = [-1.792 0.399] ^{T} mm.

The calibration process in this example is straightforward the optimal values of the tuning parameters are converted to the adjustments of the design parameters in a direct manner. After the first iteration, the new design $x^{(1)}$ = [3,208 18,399] ^{T}mm has already satisfied the design specifications Figure 7.

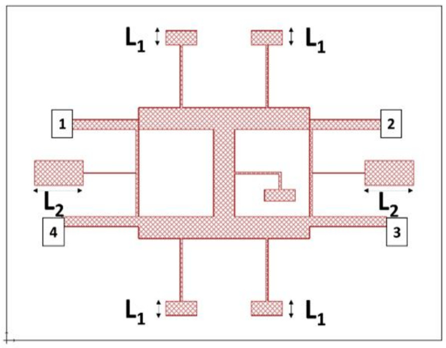

Figure 3: The Initial fine model

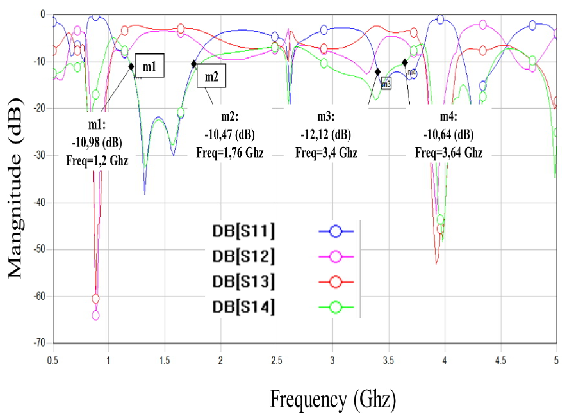

(a)

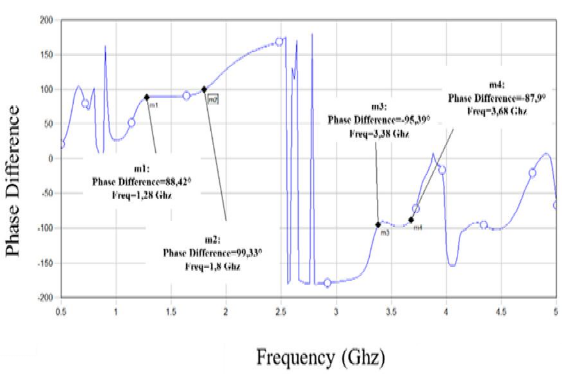

(b)

Figure. 4: The initial fine model response; **a**:S-paramertres; **b**: phase difference between Port2 and 3

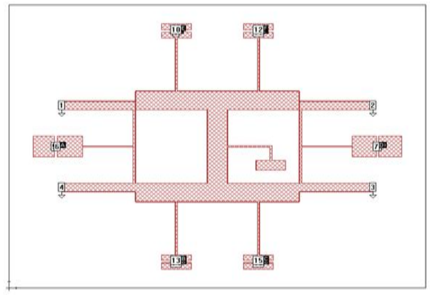

Figure 5: The fine model divided

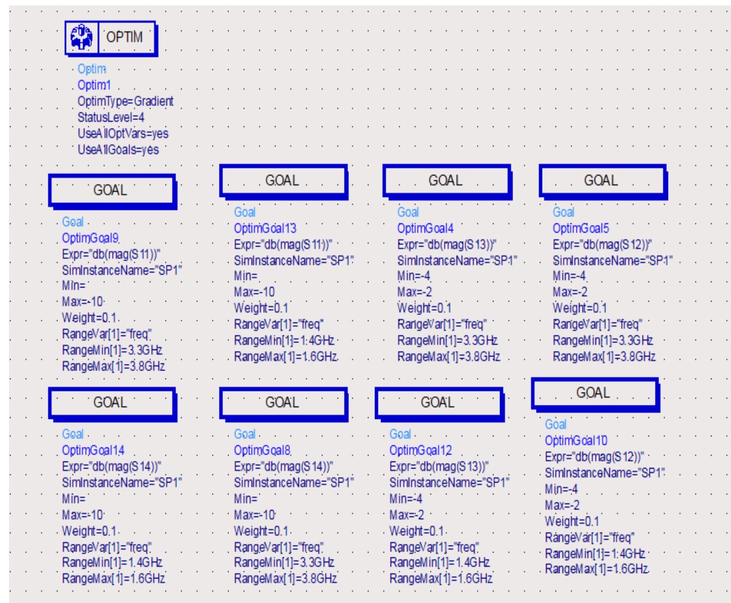

(a)

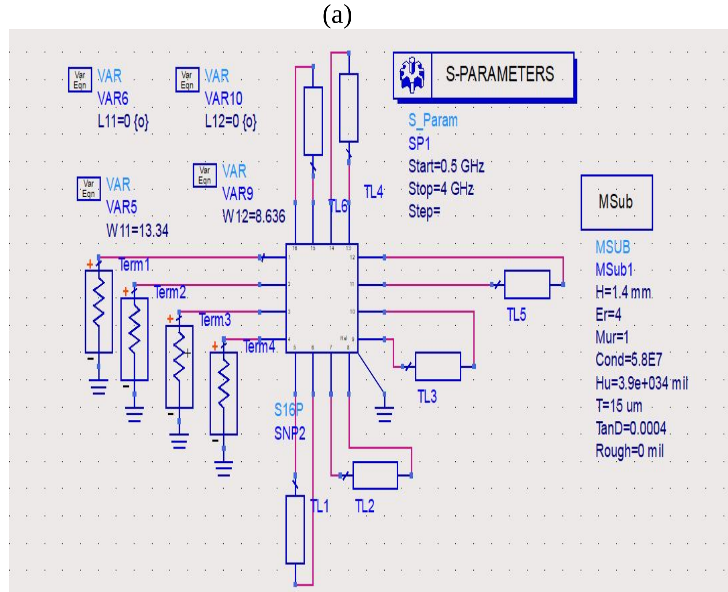

(b)

Figure 6: Fast circuit simulator design; **a**: The optimization goals; **b**: The tuning model

Figure 7 shows that after the optimization, the simulated S_{11} and S_{14} are less than -10dB within the frequency range of 1.3-1.7 GHz (first band) and within 3.4 -3.76 GHz (second band). Within a similar frequency range, the coupling coefficient is 3 ± 1 dB, the transmission coefficient is 3 ± 1 dB, and the phase difference between output ports (2 and 3) is 90 °± 5°.

Table 1 summarized the performances of this enhanced two-section dual-band BLC coupler, and a single-section one for comparison [19]. We notice that the one with two sections shows better bandwidth compared to the one with only one section. And we observe also that the optimized first band two-sections one shows better compactness that the initial one.

Table 1. Performances of the enhanced two-section and single-section dual-band BLC

Parameter	First band Two-sections (Initial)	Second Band Two-sections (Initial)	First band Two-sections (Optimized)	Second Band Two-sections (Optimized)	First band single-section [19]	Second band single-section [19]
S11 (dB)	<-10dB	<-10dB	<-10dB	<-10dB	<-10dB	<-10dB
S12 (dB)	3 ± 1 dB	3 ± 1 dB	3 ± 1 dB	3 ± 1 dB	3 ± 1 dB	3 ± 1 dB
S13 (dB)	3 ± 1 dB	3 ± 1 dB	3 ± 1 dB	3 ± 1 dB	3 ± 1 dB	3 ± 1 dB
S14 (dB)	<-10dB	<-10dB	<-10dB	<-10dB	<-10dB	<-10dB
Phase difference	90° ± 5°	90° ± 5°	90° ± 5°	90° ± 5°	90° ± 10°	90° ± 10°
Operating frequency (GHz)	1.3-1.7	3.4 -3.64	1.3-1.7	3.4 -3.76	0.8-0.92	1.88-2
Bandwidth	26.66 %	8 %	26.66 %	8.5 %	13.95 %	6.18 %
Size (mm×mm)	139.7×102.1	139.7×102.1	140.5×98.56	140.5×98.56	179×184.1-	179×184.1-

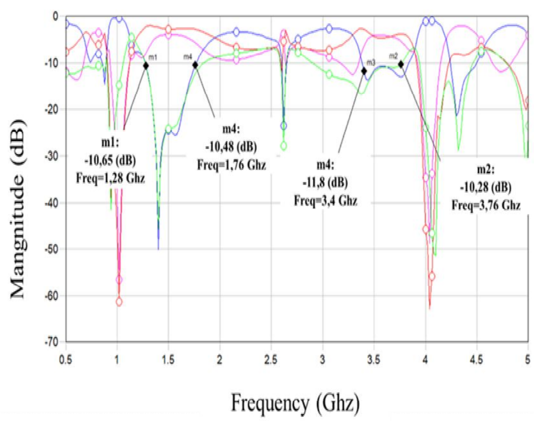

(a)

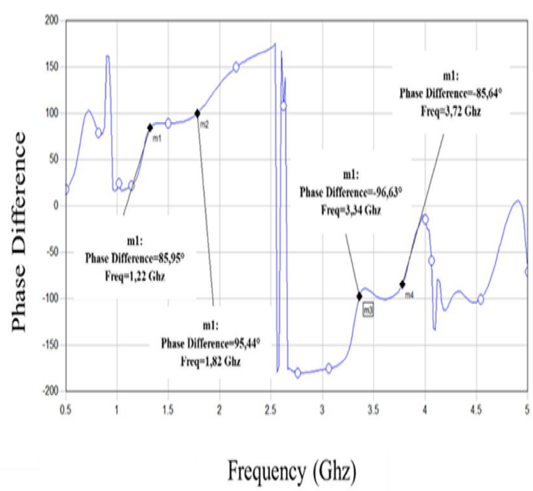

(b)

Figure 7: The optimized fine model response; **a**:S-paramertres; **b**: phase difference between Port2 and 3

5. CONCLUSION

In this work, an optimization of a two-section dual-band branch-line coupler with stepped-impedance-stub lines has been done, using an adjusted Tuning Space Mapping, the adjustment is made in the tuning model using our engineering expertise and knowledge of the design problem. The effect of using this technique has been observed as the results show that the design specifications are achieved after only three EM simulations, this is very significant considering how very low the CPU and time consumption.

REFERENCES

1. ***3GPP specification series: 38series***. Retrieved 2020-06-28,from www.3gpp.org/DynaReport/38-series.htm
2. D. M. Pozar. ***Microwave Engineering***, 4th ed. New York: Wiley , 2012.
3. M.-J. Park and B. Lee. **Dual-band, cross coupled branch line coupler**. *IEEE Microw. Wireless Compon. Lett.*, vol. 15, no. 10, pp. 655–657 , 2005.
4. I.-H. Lin, M. DeVincentis, C. Caloz, and T. Itoh. **Arbitrary dual-band components using composite right/left-handed transmission lines**.*IEEE Trans. Microw. Theory Tech.*, vol. 52, no. 4, pp. 1142–1149. 2004.
5. J.-X. Niu and X.-L. Zhou. **A novel dual-band branch line coupler based on strip-shaped complementary**

split ring resonators, *Microw. Opt. Technol. Lett*., vol. 49, no. 11, pp. 2859–2862 ,2007.
6. K.-K. M. Cheng and F.-L.Wong.**A novel approach to the design and implementation of dual-band compact planar 90 branch-line coupler**. *IEEE Trans. Microw. Theory Tech*., vol. 52, no. 11, pp. 2458–2463, 2004.
7. C. Collado, A. Grau, and F. D. Flaviis. **Dual-band planar quadrature hybrid with enhanced bandwidth response**. *IEEE Trans. Microw. Theory Tech*., vol. 54, no. 1, pp. 180–188, 2006.
8. K.-K. M. Cheng and F.-L. Wong. **Dual-band rat-race coupler design using tri-section branch-line**. *Electron. Lett.*, vol. 43, no. 6, pp. 41–42 , 2007.
9. C.-L. Hsu, J.-T. Kuo, and C.-W. Chang. **Miniaturized dual-band hybrid couplers with arbitrary power** division ratios, *IEEE Trans. Microw. Theory Tech*., vol. 57, no. 1, pp. 149–156, 2009.
10. K.-S Chin, K.-M. Lin, Y.-H. Wei, T.-H. Tseng, and Y.-J. Yang. **Compact Dual-Band Branch-Line and Rat-Race Couplers with Stepped-Impedance-Stub Lines**. *Trans. Microw. Theory Tech*, vol.58, n. 5, 2010.
11. V. Rizzoli. **Circuit-level nonlinear/electromagnetic co-simulation of an entire microwave link**, in IEEE MTT-S Int. Microwave Symp. Digest, Long Beach, CA, 2005, pp. 813–816.
12. A.I.J. Forrester, and A.J. Keane. **Recent advances in surrogate-based optimization**, *Progr. Aerosp. Sci*., vol.45, no.1, pp. 50–79, 2009.
13. J.W. Bandler, Q.S. Cheng, S.A. Dakroury, et al. **Space mapping: the state of the art**, *IEEE Trans. Microw. Theory Tech*., vol. 52, no. 1, pp. 337–361, 2004.
14. D. Echeverria, P.W. Hemker. **Space mapping and defect correction**, in *Mathematics in Industry*, pp. 107–136, 2005.
15. J. Meng, S. Koziel, J.W. Bandler, M.H. Bakr, and Q.S. Cheng. **Tuning space mapping: a novel technique for engineering design optimization**, in *IEEE MTT-S Int. Microwave Symp. Digest*, Atlanta, GA, 2008, pp. 991–994.
16. D.G. Swanson, and R.J. Wenzel, **Fast analysis and optimization of combline filters using FEM**, in *IEEE Int. Microwave Symp. Digest*, Boston:MA, 2001, pp. 1159–1162
17. J.W. Bandler, Q.S. Cheng, S.A. Dakroury, A.S. Mohamed, M.H. Bakr, K. Madsen, and J Søndergaard. **Space mapping: the state of the art**, *IEEE T. Microw. Theory*, pp.337–361, 2004.
18. A. SAADI, and S. Bri. **Non-Linear Optimization of Small Size Microwave Directional Coupler Design Using Implicit Space**, *International Journal of Microwaves Applications*, Vol.2, 2013.
19. A. El Berbri, A. Saadi, and S. Bri. **Design and Optimization of Dual-Band Branch-Line Coupler with Stepped-Impedance-Stub for 5G Applications**, *Advances in Science, Technology and Engineering Systems Journal*, vol. 5, no. 3, pp. 355-360, 2020.
20. A. El Berbri, A. Saadi, and S. Bri. **Optimized Design of Two Section Branch Line Coupler for Future 5G Applications**, *International Journal of Microwave and Optical Technology*, vol. 15, no. 1, pp. 44-50, 2020.
21. Y. Mohapatra, and M. Ray. **Hybrid Model for Cross Project Fault Prediction Using Random Forests and Multi-Objective Ant Lion Optimization,** *International Journal of Advanced Trends in Computer Science and Engineering*, vol. 8, no. 3, pp. 836-846, 2019 https://doi.org/10.30534/ijatcse/2019/78832019
22. S. N. Z. Ahmmad, and F. Muchtar. **A Review on Applications of Optimization Using Bat Algorithm,** *International Journal of Advanced Trends in Computer Science and Engineering*, vol. 9, no. 1.1, pp. 212- 219, 2020.
https://doi.org/10.30534/ijatcse/2020/3791.12020
23. S. G. Shareef , and A. L. Ibrahim. **A New Quasi-Newton (SR1) With PCG Method for Unconstrained Nonlinear Optimization**, *International Journal of Advanced Trends in Computer Science and Engineering*, vol. 8, no. 6, pp. 3124-3128, 2020.
https://doi.org/10.30534/ijatcse/2019/74862019